A Riemann Solver for Wet/Dry Interfaces in Finite volume schemes

Mathematics behind the Artifact

Name: Brian KYANJO Supervisor: Prof. Donna Calhoun

Committee: Prof. Jodi Mead, Michal Kopera, and Dylan Mikesell Date: October 24, 2021

1 Riemann solvers

Riemann solvers are the numerical method in which time-averaged fluxes of all conserved quantities are calculated to solve fundamental problems in conservation laws named Riemann problems. A Riemann problem can be defined as a specific initial value problem (Cauchy) of a partial differential equation (PDE) that consists of conservation equations (1) combined with piece-wise constant initial data which has a single discontinuity in the domain of interest as shown in equation (2) [George, 2011].

$$q_t + f(q)_x = 0 \tag{1}$$

$$q(x,0) = \begin{cases} q_L, & \text{if} \quad x \leq 0, \\ q_R, & \text{if} \quad x > 0, \end{cases} \tag{2}$$

where $f(q)_x \in \mathbb{R}^m$ is a vector of conserved quantities, q_R and q_L are two piece-wise constant states separated by a discontinuity.

2 Shallow Water Equations (SWE)

The SWE are a system of hyperbolic PDEs governing the flow below a pressure surface in a fluid. They arise from the Navier-Stokes equations. In one dimension, the SWE can be used to model a fluid in a channel of unit width, taking the vertical velocity negligible, and horizontal velocity roughly constant throughout any cross section of the channel George [2008].

Consider small-amplitude waves in a one-dimensional fluid channel that is shallow relative to its wavelength. The conservation of momentum equation is written in terms of pressure, $p(x,t) = \frac{1}{2}\rho g h^2$, and the height field $h(x,t)$ (m), which breaks down into system (3).

$$\begin{aligned} h_t + (uh)_x &= 0 \\ (hu)_t + \left(hu^2 + \frac{1}{2}\rho g h^2\right)_x &= 0 \end{aligned} \tag{3}$$

where hu measures the flow rate of water past a point, ρ (kg/m^3) is the constant density of the incompressible fluid, and $u(x,t)$ (m/s) is the horizontal velocity. We will set $\rho = 1$ here.

A very simple set of initial conditions is a single discontinuity at the middle of the channel. In this case, we set h and hu equal to constants on either side of the channel. This problem is a classic Riemann Problem, and for the SWE, has an exact solution. We assume the discontinuity is at $x = 0$. The variation of h and hu on either side of the discontinuity leads the waves in the Riemann problem to move at different speeds creating discontinuities (shocks) or changing regions (rarefactions) LeVeque et al. [2002]. At $x = 0$ and $t = 0$, the discontinuity is located between the left and right state, so the solution at the left $(q_l)$and right(q_r) states are given by:

$$q_l = \begin{bmatrix} h_l \\ (hu)_l \end{bmatrix} \quad \text{and} \quad q_r = \begin{bmatrix} h_r \\ (hu)_r \end{bmatrix} \tag{4}$$

As t increases, four distinct regions are created, separated by characteristics. The middle state called the intermediate state(q_m), is generated. The determination of this state characterizes the Riemann problem and how it connects to other states via waves in each respective characteristic family Bale et al. [2003]. This can only hold if the connection wave speeds satisfy the Lax entropy condition. Figure 1 shows a wave combination of a centered rarefaction and shock wave from the first and second characteristic family respectively.

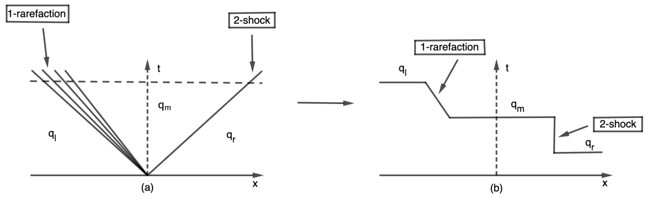

Figure 1: x-t plane showing the connection of states, 1-rarefaction fan, and the 2-shock.

The intermediate state is obtained by solving the Riemann problem using the exact or approximate method. Approximate methods are widely used due to their cheap computational cost compared to the exact solvers.

2.1 Exact Riemann Solver for two-shock SWE

The states in 1 are separated by either *shocks* or *rarefactions*. General left and right states will be connected by a combination of the two (either two shocks, two rarefactions, or one of each). We describe how to determine if two states are connected by a shock. We refer the reader to LeVeque et al. [2002] for other cases.

We can obtain an exact solution to the Riemann Problem for the SWE as follows. The shock speed, $s(t)$, from the shock wave as the solution emerges is determined from the Rankine-Hugoniot jump condition given by equation (5) which must be satisfied across any shock wave. If q_l and q_r are connected by a shock, the Rankine Hugoniot conditions will be satisfied Mandli et al. [2016].

$$\begin{aligned} s_1(q_m - q_l) &= f(q_m) - f(q_l) \\ s_2(q_r - q_m) &= f(q_r) - f(q_m) \end{aligned} \tag{5}$$

By applying condition (5) to shallow water equations (3) creates a system of four equations (6) that must be satisfied simultaneously.

$$\begin{aligned} s_1(h_m - h_l) &= hu_m - hu_l \\ s_1(hu_m - hu_l) &= hu_m^2 - hu_l^2 + \frac{1}{2}g(h_m^2 - h_l^2) \\ s_2(h_r - h_m) &= hu_r - hu_m \\ s_1(hu_r - hu_m) &= hu_r^2 - hu_m^2 + \frac{1}{2}g(h_r^2 - h_m^2) \end{aligned} \tag{6}$$

Since the (h_l, u_l) and (h_r, u_r) are fixed, we find all states: (h_m, u_m) and their corresponding speeds: s_1 and s_2 that satisfy system (6). We have four equations and four unknowns, which gives a two parameter family of solutions: one-shock and two-shock. Using h_l and h_r as parameters, corresponding u_l, u_r, s_1,and s_2 are determined for each h_l and h_r. And then a graph of hu against h is plotted that gives the curves in fig. 2. The point of intersection between the *1-shock (blue)* and *2-shock (orange)* physical solutions is the intermediate state q_m. The dotted curves represent unphysical solution LeVeque et al. [2002].

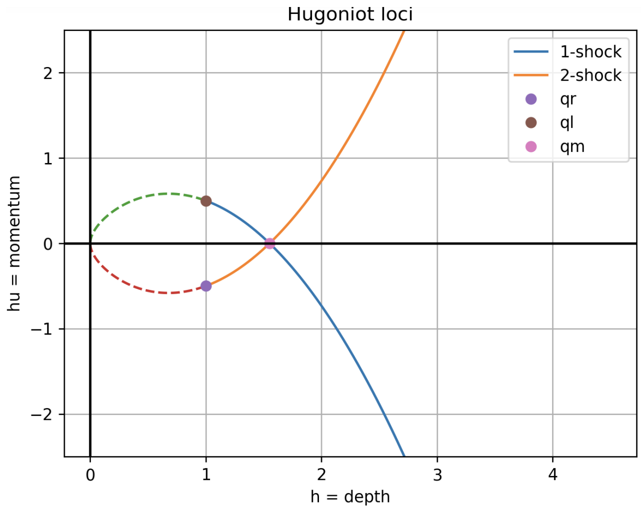

Figure 2: Shows curves that represent all states connected to q_l and all states connected to q_r via a *2-shock* and *1-shock* respectively. Equations (7) and (8) are solved to produce the curves.

Consider a general Riemann problem whose known solution consists of two shocks with initial data (4). This problem can be solved by finding the state q_m that can be connected to q_l by a *1-shock* and simultaneously connects to q_r by a *2-shock*. The point q_m lies on the curve (7) of points through point q_r that connects to q_r by a *2-shock* Berger et al. [2011].

$$u_m = u_r + (h_m - h_r)\sqrt{\frac{g}{2}\left(\frac{1}{h_m} + \frac{1}{h_r}\right)} \tag{7}$$

Likewise, the state(q_m), must also lie on the Hugonoit locus (equation (8)) of the 1-shock wave passing through q_l

$$u_m = u_l - (h_m - h_l)\sqrt{\frac{g}{2}\left(\frac{1}{h_m} + \frac{1}{h_l}\right)} \tag{8}$$

Equations (7) and (8) form a system of two equations with two unknowns (h_m and u_m) that are equated since the left-hand sides of both equations are equal. A non linear equation that consist of only one unknown h_m is formed and solved using an iterative method such as Newton method to obtain a desired intermediate state in the Riemann solution LeVeque et al. [2011].

As an example, consider a SWE Riemann problem with $h_l = h_r = 1, u_l = 0.5$, and $u_r = -0.5$. These initial values are used by the Newton solver to solve equations (7) and (8) to produce $h_m = 1.554$. The shock speeds (s_l and s_r) in each region are different due to different wave characteristics, we use this concept to loop through all interfaces and determine h and hu in each region as shown in the code 1 . At each interface the function *Riemann_solution*, is called and respective values of height (h) and momentum (hu) solutions are stored. According to Lax entropy conditions, a *1-shock* that physically connects q_l to q_m is obtained if $h_m > h_l$, and similarly a *2-shock* wave that physically connects q_m to q_r requires $h_m > h_r$ LeVeque et al. [2011].

```
def Riemann_solution(ql,qr,qm,xi,g)    # xi = x/t
qm = array([hm,hum])    # intermediate state
sl = lambda h,ql: ql[1]/ql[0] - (1/ql[0] )*sqrt((g/2)*(ql[0]*h*(ql[0]+h)))
sr = lambda h,qr: qr[1]/qr[0] - (1/qr[0] )*sqrt((g/2)*(qr[0]*h*(qr[0]+h)))
if 0.5*(sl(hl,ql) + sl(hm,qm)) > xi : # left to middle state
h = hl
u = ul
hu = h*u
elif sl(hm,qm) < xi and xi < sr(hm,qr): # middle state
h = hm
u = um
hu = h*u
else:     # middle to right state
h = hr
```

```python
    u = ur
    hu = h*u
    return h, hu

```

Listing 1: Python code describing how the two shock case solution is obtained after the first time step.

The height field solution h obtained from the code 1 above is plotted in fig. 3. The plot depicts the left region being connected to the middle region via a *1-shock* wave and the middle being connected to the right region via a a *2-shock* wave.

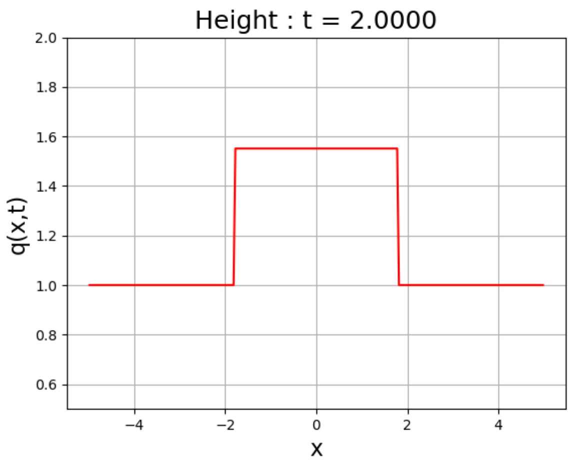

Figure 3: Shows all-shock Riemann exact solution

3 Finite volume discretization

Consider a one dimensional (1D) conservation law (equation (9)), where q is the measure of conserved quantity density and $f(q)$ is a flux function George [2011].

$$q_t(x,t) + f(q(x,t))_x = 0 \tag{9}$$

In finite volume methods (FVM), the domain is broken down into grid cells. Consider $C_i = (x_{i-\frac{1}{2}}, x_{i+\frac{1}{2}})$ to be the i^{th} grid cell, the average value over the i^{th} interval at time t^n is numerically approximated by Q_i^n in equation (10).

$$Q_i^n \approx \frac{1}{\Delta x}\int_{C_i} q(x,t^n)dx \tag{10}$$

where $\Delta t = (t^{n+1} - t^n)$ and $\Delta x = (x_{i+\frac{1}{2}} - x_{i-\frac{1}{2}})$ is the cell length. A discontinuity in q violates the PDE in the classical sense and only holds for the integral conservation law (fundamental equation (11)) LeVeque et al. [2002]. Therefore at grid points near discontinuities where PDEs don't hold, all classical finite difference methods breakdown, resorting to FVM which are based on (11).

$$\frac{d}{dt}\int_{c_i} q(x,t)dx = f(q(x_{i-\frac{1}{2}},t)) - f(q(x_{i+\frac{1}{2}},t)) \tag{11}$$

The approximate total integral of q over each grid cell is evaluated and updated at every time step by the grid cell edge fluxes. The determined numerical flux functions evaluate the cell averages over a certain volume, which are used to approximate the solutions within the cells, using equation (12) LeVeque et al. [2011].

$$Q_i^{n+1} = Q_i^n - \frac{\Delta t}{\Delta x}(F^n_{i+\frac{1}{2}} - F^n_{i-\frac{1}{2}}) \tag{12}$$

where $F^n_{i+\frac{1}{2}}$ is the average flux approximation along $x = x_{i-\frac{1}{2}}$. The Riemann problem is a fundamental tool in the evolution of FVM. Taking two neighbouring grid cells: $Q_{i-1} = q_L$ and $Q_i = q_R$ to be cell averages, this information is used by the exact Riemann solver to compute numerical fluxes ($F^n_{i-\frac{1}{2}} = \mathcal{F}(Q_{i-1}, Q_i)$), that are used to update the cell average at each time step Bale et al. [2003]. Then equation (12) becomes:

$$Q_i^{n+1} = Q_i^n - \frac{\Delta t}{\Delta x}\left[\mathcal{F}(Q_i, Q_{i+1}) - \mathcal{F}(Q_{i-1}, Q_i)\right] \tag{13}$$

where $\mathcal{F}$ is some numerical flux function.

4 Wave Propagation Algorithm (WPA)

Equation (12), can be reformulated as a first order wave propagation method by decomposing flux at the cell averages into fluctuations ($\mathcal{A}^+\Delta Q^n_{i-\frac{1}{2}}$ and $\mathcal{A}^- Q^n_{i+\frac{1}{2}}$) as shown in equations (14) and (15) Mandli et al. [2016].

$$\mathcal{A}^+\Delta Q^n_{i-\frac{1}{2}} = f(Q_i) - f(Q^*_{i-\frac{1}{2}}) \tag{14}$$

$$\mathcal{A}^-\Delta Q^n_{i+\frac{1}{2}} = f(Q^*_{i+\frac{1}{2}}) - f(Q_i) \tag{15}$$

where $\mathcal{A}^+\Delta Q^n_{i-\frac{1}{2}}$ and $\mathcal{A}^- Q^n_{i+\frac{1}{2}}$ are the net updating contributions from the rightward and leftward moving waves into the grid cell C_i from the right and left interface respectively, $Q^*_{i-\frac{1}{2}}$ is the intermediate cell average determined by the exact Riemann solver at $x_{i-\frac{1}{2}}$, and $f(Q^*_{i-\frac{1}{2}})$ is numerical flux at $Q^*_{i-\frac{1}{2}}$ George [2008]. Combining equations (14) and (15), the first order 1D wave propagation method is given by equation (16).

$$Q_i^{n+1} = Q_i^n - \frac{\Delta t}{\Delta x}(\mathcal{A}^+\Delta Q^n_{i-\frac{1}{2}} + \mathcal{A}^- Q^n_{i+\frac{1}{2}}) \tag{16}$$

The general conservation law in (9) can be written in *quasi-linear form* as

$$q_t + f'(q)q_x = 0 \tag{17}$$

where $f'(q) \in \mathbb{R}^{m\times m}$ flux Jacobian matrix. Consider a Riemann problem for the system (17) with initial data

$$q(x, t^n) = \begin{cases} Q^n_{i-1} & \text{if} \quad x < x_{i-\frac{1}{2}} \\ Q^n_i & \text{if} \quad x > x_{i-\frac{1}{2}} \end{cases} \tag{18}$$

The initial data (equation (18)), is used by the exact Riemann solver to generate an intermediate state ($q_m = (h_m, hu_m)^T$), which is used to evaluate the eigenvalues ($\lambda_{i-1/2}$) and eigenvectors ($r_{i-1/2}$) at $x = x_{i-\frac{1}{2}}$. The p^{th} wave at interface $i - 1/2$ is given by $\mathcal{W}^p_{i-1/2} \equiv \alpha_{i-\frac{1}{2}} r^p_{i-\frac{1}{2}}$ with speeds $s^p_{i-1/2} = \lambda^p_{i-1/2}$ LeVeque et al. [2002]. where $\alpha_{i-\frac{1}{2}}$ depicts the coefficients of the the eigenvectors. Waves and speeds are obtained as an eigenvector decomposition of the jump in Q_i at the interface $i - \frac{1}{2}$. This decomposition takes the form

$$Q_i - Q_{i-1} = \sum_{p=1}^{m} \alpha_{i-\frac{1}{2}} r_{i-\frac{1}{2}} \tag{19}$$

The wave speed $s^p_{i-\frac{1}{2}}$ associated with the vector $r^p_{i-\frac{1}{2}}$, are preselected basing on the characteristic structure of the initial Riemann data George [2008]. Therefore the fluctuations $\mathcal{A}^+\Delta Q^n_{i-\frac{1}{2}}$ and $\mathcal{A}^-\Delta Q^n_{i-\frac{1}{2}}$ are defined by equations (20) and (21):

$$\mathcal{A}^-\Delta Q^n_{i-\frac{1}{2}} = \sum_{\{p:s^p_{i-\frac{1}{2}}<0\}} s^p_{i-\frac{1}{2}}\mathcal{W}^p_{i-\frac{1}{2}} \tag{20}$$

$$\mathcal{A}^+\Delta Q^n_{i-\frac{1}{2}} = \sum_{\{p:s^p_{i-\frac{1}{2}}>0\}} s^p_{i-\frac{1}{2}}\mathcal{W}^p_{i-\frac{1}{2}} \tag{21}$$

In a standard conservative case ((9)), the sum of the left-going and right-going fluctuations should satisfy:

$$\mathcal{A}^+\Delta Q^n_{i-\frac{1}{2}} + \mathcal{A}^- Q^n_{i+\frac{1}{2}} = f(Q_i) - f(Q_{i-1}) \tag{22}$$

The second order accuracy is obtained by taking the correction terms into account as shown described in equation (23) Barzgaran et al. [2019]

$$Q_i^{n+1} = Q_i^n - \frac{\Delta t}{\Delta x}(\mathcal{A}^+\Delta Q^n_{i-\frac{1}{2}} + \mathcal{A}^- Q^n_{i+\frac{1}{2}}) - \frac{\Delta t}{\Delta x}(\tilde{F}^n_{i+\frac{1}{2}} - \tilde{F}^n_{i-\frac{1}{2}}) \tag{23}$$

where $\tilde{F}^n_{i-\frac{1}{2}}$ are second order correction terms determined by the waves and speeds in the Riemann problems after approximating the average flux along $x = x_{i-\frac{1}{2}}$:

$$\tilde{F}^n_{i-\frac{1}{2}} = \frac{1}{2}\sum_{p=1}^{m} |s^p_{i-\frac{1}{2}}| \left(1 - \frac{\Delta t}{\Delta x}|s^p_{i-\frac{1}{2}}|\right) \tilde{\mathcal{W}}^p_{i-\frac{1}{2}} \tag{24}$$

Here $\tilde{\mathcal{W}}^p_{i-\frac{1}{2}}$ depicts a limited version of the wave $\mathcal{W}^p_{i-\frac{1}{2}}$, which is obtained after a comparison between $\mathcal{W}^p_{i-\frac{1}{2}}$ and $\mathcal{W}^p_{i-\frac{3}{2}}$ when $s^p > 0$ Bale et al. [2003].

4.1 WPA for the Shallow Water Equations

The combination of equations in system (3), forms a system of one-dimensional SWEs given by equation (25)

$$\begin{bmatrix} h \\ hu \end{bmatrix}_t + \begin{bmatrix} uh \\ hu^2 + \frac{1}{2}gh^2 \end{bmatrix}_x = 0 \tag{25}$$

Equation (25) can be written as a quasi-linear system as shown in equation (26):

$$\begin{bmatrix} h \\ hu \end{bmatrix}_t + \begin{bmatrix} 0 & 1 \\ -u^2 + gh & 2u \end{bmatrix} \begin{bmatrix} h \\ hu \end{bmatrix}_x = \begin{bmatrix} 0 \\ 0 \end{bmatrix} \tag{26}$$

where the flux Jacobian matrix $f'(q)$ is given by

$$f'(q) = \begin{bmatrix} 0 & 1 \\ -u^2 + gh & 2u \end{bmatrix} \tag{27}$$

The non linear problem (equation (9)), can be replaced by a linearized problem defined locally at each cell interface LeVeque et al. [2011],

$$\hat{q}_t + \hat{A}_{i-\frac{1}{2}}\hat{q}_x = 0 \tag{28}$$

where 2×2 matrix $\hat{A}_{i-\frac{1}{2}}$ (equation (29)) is selected to be an approximation of $f'(q)$ that is valid in the neighbourhood of the intial data Q_{i-1} and Q_i.

$$\hat{A}_{i-\frac{1}{2}} = \begin{bmatrix} 0 & 1 \\ -\hat{u}^2 + g\bar{h} & 2\hat{u} \end{bmatrix} \tag{29}$$

where $\bar{h} = \frac{1}{2}(h_{i-1} + h_i)$ is the average between end points h_{i-1} and h_i, g is the acceleration due to gravity, and $\hat{u} = (\sqrt{h_{i-1}}u_{i-1} + \sqrt{h_i}u_i)/(\sqrt{h_{i-1}} + \sqrt{h_i})$ is the Roe average. Since $\hat{A}_{i-\frac{1}{2}}$ is a real diagonalizable Jacobian matrix evaluated at $\hat{q} = (\bar{h}, \bar{h}\hat{u})$, then its eigenvalues $(\hat{\lambda})$ and eigenvectors $(\hat{r})$ are given by equations (30) and (31) respectively LeVeque and Pelanti [2001].

$$\hat{\lambda}^1 = \hat{u} - \hat{c}, \qquad \hat{\lambda}^2 = \hat{u} + \hat{c} \tag{30}$$

$$\hat{r}^1 = \begin{bmatrix} 1 \\ \hat{\lambda}^1 \end{bmatrix}, \qquad \hat{r}^2 = \begin{bmatrix} 1 \\ \hat{\lambda}^2 \end{bmatrix} \tag{31}$$

where $\hat{c} = \sqrt{gh}$, the approximate Riemann solver is used to decompose the vector $\delta \equiv Q_i - Q_{i-1}$ into two waves: $\alpha^1_{i-\frac{1}{2}}\hat{r}^1$ and $\alpha^1_{i-\frac{1}{2}}\hat{r}^2$ as

$$Q_i - Q_{i-1} = \alpha^1_{i-\frac{1}{2}}\hat{r}^1 + \alpha^1_{i-\frac{1}{2}}\hat{r}^2 \equiv \mathcal{W}^1_{i-\frac{1}{2}} + \mathcal{W}^2_{i-\frac{1}{2}} \tag{32}$$

where the coefficients $\alpha^1_{i-\frac{1}{2}}$ are given by:

$$\alpha^1_{i-\frac{1}{2}} = \frac{(\hat{u} + \hat{c})\delta^1 - \delta^2}{2\hat{c}} \tag{33}$$

$$\alpha^2_{i-\frac{1}{2}} = \frac{-(\hat{u} - \hat{c})\delta^1 + \delta^2}{2\hat{c}} \tag{34}$$

5 Limiters

Accuracy of smooth solutions are obtained by advancing first order methods to second order accurate, but these still fail at the neighbourhood of discontinuities, where oscillations (noise) are created. Limiters use the characteristics of the solution at such regions to filter out the oscillations eliminating the phase error hence increasing accuracy. The second order correction terms are computed basing on several different families of waves produced by the Riemann solution, the superposition of such waves make limiting process very difficult George [2011] . Since in some regions, some waves may be discontinuous while others are smooth, therefore different limiter types handle this process in a different way, making some limiters to perform better than others depending on the method they are applied too Berger et al. [2011].

The Dispersive nature of some methods may produce oscillations even in smooth solutions. During the simulations we focused on using only four high-resolution limiters: minmod, superbee, MC, and van Leer.

$$\text{minmod}: \ \phi(\theta) = \text{minmod}(1, \theta) \tag{35}$$

$$\text{MC}: \ \phi(\theta) = \max\left(0, \frac{\min(1+\theta)}{2}, 2, 2\theta\right) \tag{36}$$

$$\text{superbee}: \ \phi(\theta) = \max(0, \min(1, 2\theta), \min(2, \theta)) \tag{37}$$

$$\text{van Leer}: \ \phi(\theta) = \frac{\theta + |\theta|}{1 + |\theta|} \tag{38}$$

where $\phi(\theta)$ is a limiter function. Each limiter behaved differently in phasing out oscillations, even though the simple limiter (minmod), performed better in filtering out the noise near the 2-shock for the flux formulation method as shown in fig. **??**, since its a slope limiter that lies along the lower boundary of the Sweby region in the θ-ϕ plane. Full second order accuracy is obtained for MC if the function ϕ is smooth near $\theta = 1$. The van Leer is a smoother version of MC, and the superbee lies along the upper boundary of the Sweby region and it did not perform well because it gives much too compression Mandli et al. [2016].

6 Bathymetric source terms

Equation (3), can be extended to balance equations by introducing a bathymetric source term as shown in equation (39). This is done by discretising the source term to generate values $-gh_{i-\frac{1}{2}}B'(x_{i-\frac{1}{2}})$ at cell interfaces $x = x_{i-\frac{1}{2}}$. This approach is very useful, because the discrepancy caused due to the failure of the flux gradient to counterbalance the source term in a near steady state solution is decomposed into propagating waves making the approach more robust than the quasi-steady WPA [Bale et al., 2003].

$$
\begin{aligned}
h_t + (uh)_x &= 0 \\
(hu)_t + \left(hu^2 + \frac{1}{2}gh^2\right)_x &= -\,ghB'(x)
\end{aligned}
\tag{39}
$$

where $B(x)$ represents bottom elevation.

The fwaves are introduced to handle the stationery states and also solve accurately the quasi-steady problems in which the objective is to obtain propagation due to small amplitude perturbations. The standard WPA (4) is conservative if and only if equation (40) is satisfied, but the flux-based wave decomposition yields a more flexible algorithm that is conservative even when equation(40) is not satisfied. And works perfect even for problems in which the Roe average is not easily computed Bale et al. [2003].

$$A_{i-\frac{1}{2}}(Q_i - Q_{i-1}) = f(Q_i) - f(Q_{i-1}) \tag{40}$$

The flux difference $f(Q_i) - f(Q_{i-1})$ is directly decomposed as a linear combination of the eigenvectors $r_{i-\frac{1}{2}}$ as shown in equation (41) Barzgaran et al. [2019]

$$f(Q_i) - f(Q_{i-1}) - \Delta x \psi_{i-\frac{1}{2}} = \sum_{p=1}^{m} \beta^p_{i-\frac{1}{2}} r^p_{i-\frac{1}{2}} \equiv \sum_{p=1}^{m} \mathcal{Z}^p_{i-\frac{1}{2}} \tag{41}$$

where

$$\beta_{i-\frac{1}{2}} = R^{-1}_{i-\frac{1}{2}}(f(Q_i) - f(Q_{i-1})) - \Delta x \psi_{i-\frac{1}{2}} \tag{42}$$

The vectors $\mathcal{Z}^p = \beta^p r^p$ are called the fwaves, as they are similar to the waves $\mathcal{W}^p$ though they carry flux increments rather than q increments. The standard WPA (4) first and second order corrections have been advanced to capture the flux based wave decomposition by changing equations (19) and (24) to (42) and (43) respectively.

$$\tilde{F}^n_{i-\frac{1}{2}} = \frac{1}{2}\sum_{p=1}^{m} \operatorname{sgn}(s^p_{i-\frac{1}{2}})\left(1 - \frac{\Delta t}{\Delta x}|s^p_{i-\frac{1}{2}}|\right)\tilde{\mathcal{Z}}^p_{i-\frac{1}{2}} \tag{43}$$

where $\tilde{\mathcal{Z}}^p_{i-\frac{1}{2}}$ is also a limited version of the f-wave $\mathcal{Z}^p_{i-\frac{1}{2}}$, obtained in the same way as $\tilde{\mathcal{W}}^p_{i-\frac{1}{2}}$ was obtained from $\mathcal{W}^p_{i-\frac{1}{2}}$ LeVeque et al., 2011. As seen in fig. **??**, the second order correction term for the f-wave approach(wpa_flux) phased out the oscillations near discontinuities without employing any limiter compared to the Roe-solver that employed the standard WPA. This means that the stationery waves near the discontinuities have been handled by the f-wave approach.

In the previous section we discussed how the exact solver solved the Riemann problem for cases in which the water height field is strictly positive everywhere. According to Toro [2001], dry states are regions with zero water depth. In such states SWEs are not applicable, so we consider wet states adjacent to dry regions as shown in figure 4. This enables solving SWEs in wet states, right up the boundary between wet and dry states LeVeque et al. [2011].

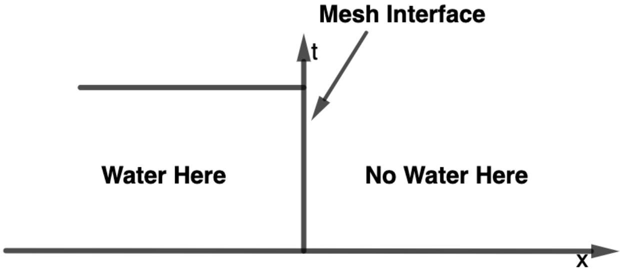

Figure 4: The Riemann problem with a dry bed (has no water) in one of the data state.

In both Barzgaran et al. [2019] and Toro [2001], there are three possible cases of wet/dry interfaces to consider as illustrated in fig. 5. Case (a) right dry bed, the solution exhibits *1-rarefaction* wave associated with the left eigenvalue $\lambda_1 = u - a$. Case (b) Left dry bed, the solution exhibits *2-rarefaction* wave associated with the right eigenvalue $\lambda_2 = u + a$. Case (c) dry bed doesn't exit at $t = 0$, but is created in the interaction between the two left and right wet bed regions if $S_{*L} \leq S_{*R}$ where $a = \sqrt{gh}$ LeVeque et al. [2011].

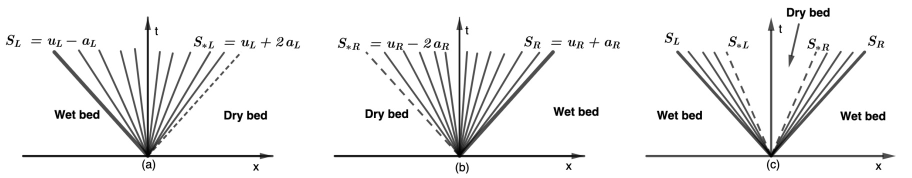

Figure 5: The dry state appears in three cases: (a) dry region is on the right, (b) dry region is on the left, and (c) dry region appears in the interaction of two wet bed states.

Here, we describe the approach taken by George [2008]. LeVeque and Pelanti [2001] proposed that equation (25) can be decomposed into equation (44):

$$\begin{bmatrix} H_i - H_{i-1} \\ HU_i - HU_{i-1} \\ \varphi(Q_i) - \varphi(Q_{i-1}) \end{bmatrix} = \sum_{p=1}^{3} \alpha^p_{i-\frac{1}{2}} w^p_{i-\frac{1}{2}} \tag{44}$$

where the momentum flux $\varphi(q) = (hu^2 + \frac{1}{2}gh^2)$, $Q_i = (H_i, HU_i)^T$ represents the numerical solution of $q = (h, hu)^T$ in C_i, and $w^p_{i-\frac{1}{2}} \in \mathbb{R}^3$,$\forall\ p \in [1, 3]$ with p a set of chosen independent vectors.

The decomposition of the solutions $Q_i - Q_{i-1}$ and $f(Q_i) - f(Q_{i-1}) \in \mathbb{R}^2$ are represented by the first two and last two components of the three components of the decomposition (44) respectively. Conservation is maintained by modifying fluctuations using the last two of the three components in equation (44) Bale et al. [2003]. Then consider $z^p_{i-\frac{1}{2}} \in \mathbb{R}^2$ for each $p \in [1, 3]$ to be flux waves defined by:

$$z^p_{i-\frac{1}{2}} = [\mathbf{0}_{2\times 1} \quad \mathbf{I}_{2\times 2}]\alpha^p_{i-\frac{1}{2}} w^p_{i-\frac{1}{2}} \tag{45}$$

where $\mathbf{0}_{2\times 1}$ is a two by one zeros matrix, $\mathbf{I}_{2\times 2}$ is a two by two identity. Then updated fluctuations become:

$$\mathcal{A}^+ \Delta Q^n_{i-\frac{1}{2}} = \sum_{\{p: s^p_{i-\frac{1}{2}} > 0\}} z^p_{i-\frac{1}{2}} \tag{46}$$

$$\mathcal{A}^- \Delta Q^n_{i+\frac{1}{2}} = \sum_{\{p: s^p_{i+\frac{1}{2}} < 0\}} z^p_{i+\frac{1}{2}} \tag{47}$$

Equations 46 and 47 are determined by decomposing flux in a similar way as in the f-wave approach in Bale et al. [2003] and George [2006], however in George [2008] its decomposed into three waves

($w^p_{i-\frac{1}{2}} \in \mathbb{R}^3$) with three associated wave speeds ($s^p_{i-\frac{1}{2}}$ for $p = 1, 2, 3$) rather than two allowing a more accurate approximation to the Riemann problem with a large rarefaction and a natural entropy fix for transonic rarefactions. The first and third eigen pairs $\{w^{1,3}_{i-\frac{1}{2}}, s^{1,3}_{i-\frac{1}{2}}\}$ are related to the eigen pairs of (27), even though in Berger et al. [2011], its the first and second pairs that relate to the original fields of SWE.

Therefore from the three eigen pairs, we choose,

$$\begin{aligned}\{w^1_{i-\frac{1}{2}}, s^1_{i-\frac{1}{2}}\} &= \{(1, \check{s}^-_{i-\frac{1}{2}}, (\check{s}^-_{i-\frac{1}{2}})^2)^T, \check{s}^-_{i-\frac{1}{2}}\}\\ \{w^3_{i-\frac{1}{2}}, s^3_{i-\frac{1}{2}}\} &= \{(1, \check{s}^+_{i-\frac{1}{2}}, (\check{s}^+_{i-\frac{1}{2}})^2)^T, \check{s}^+_{i-\frac{1}{2}}\}\end{aligned} \tag{48}$$

where $\check{s}^\pm_{i-\frac{1}{2}}$ are the Einfeldt speeds Barzgaran et al. [2019], George [2008], Berger et al. [2011] defined by:

$$\begin{aligned}\check{s}^-_{i-\frac{1}{2}} &= \min(\lambda^-(Q^n_{i-1}), \hat{\lambda}^-_{i-\frac{1}{2}})\\ \check{s}^+_{i-\frac{1}{2}} &= \max(\lambda^+(Q^n_i), \hat{\lambda}^+_{i-\frac{1}{2}})\end{aligned} \tag{49}$$

where $\lambda^\pm = u \pm \sqrt{gh}$ are eigen values of equation (27) and $\check{\lambda}^\pm_{i-\frac{1}{2}}$ are eigen values of the Roe averaged Jacobian matrix $\hat{A}_{i-\frac{1}{2}}$ in equation (29). The second pair $\{w^2_{i-\frac{1}{2}}, s^2_{i-\frac{1}{2}}\}$ that result into the second wave named corrector wave and speed is arbitrary chosen in various ways. The corrector wave corrects inaccurate, non-conservative and entropy violating approximate Riemann solutions with only two waves Berger et al. [2011].

There is only one rarefaction in the exact Riemann solution, that connects wet to dry state. The developing wet/dry interface is in this case single edge of the rarefaction, making it possible to determine the interface propagating speed using the corresponding characteristics field of the Riemann invariants LeVeque et al. [2011]. In George [2006] and George [2008], Einfeldt speeds ((49)) define two propagating discontinuities, the middle state between them is determined to maintain conservation and its depth at interface $x_{i-\frac{1}{2}}$ is given by:

$$\check{H}^*_{i-\frac{1}{2}} = \frac{HU_{i-1} - HU_i + \check{s}^+_{i-\frac{1}{2}} H_i - \check{s}^-_{i-\frac{1}{2}} H_{i-1}}{\check{s}^+_{i-\frac{1}{2}} - \check{s}^-_{i-\frac{1}{2}}} \tag{50}$$

The wet/dry interface propagation speed is given by equation (51), since the right state in figure 4, is considered as the initial dry state, which also makes the rarefaction to be in the first characteristic field as shown in figure 5.(a) George [2008].

$$s^3_{i-\frac{1}{2}} = \check{s}^+_{i-\frac{1}{2}} = \lambda^{-*}_{i-\frac{1}{2}}(H^*_{i-\frac{1}{2}} = 0) = U_{i-1} - 2\sqrt{gH_{i-1}} \tag{51}$$

If the left state in figure 4, is considered as the initial dry state, then the wet/dry interface propagation speed is given by equation (52), and the rarefaction is in the second characteristic field as shown in figure 5.(b) George [2008].

$$s^1_{i-\frac{1}{2}} = \check{s}^-_{i-\frac{1}{2}} = \lambda^{+*}_{i-\frac{1}{2}}(H^*_{i-\frac{1}{2}} = 0) = U_i - 2\sqrt{gH_i} \tag{52}$$

Note that the middle state depth $H^*_{i-\frac{1}{2}} = 0$ since it corresponds to the initial dry state

References

J Comp Phys.

E. Audusse, F. Bouchut, M.-O. Bristeau, R. Klein, and B. t. Perthame. A fast and stable well-balanced scheme with hydrostatic reconstruction for shallow water flows. *SIAM Journal on Scientific Computing*, 25(6):2050–2065, 2004.

D. Bale, R. J. LeVeque, S. Mitran, and J. Rossmanith. A Wave Propagation Method for Conservation Laws and Balance Laws with Spatially Varying Flux Functions. 24(3):955–978, 2003. doi: 10.1137/S106482750139738X. URL http://dx.doi.org/10.1137/S106482750139738X.

M. Barzgaran, H. Mahdizadeh, and S. Sharifi. Numerical simulation of bedload sediment transport with the ability to model wet/dry interfaces using an augmented riemann solver. *Journal of Hydroinformatics*, 21(5):834–850, 2019.

M. J. Berger, D. L. George, R. J. LeVeque, and K. T. Mandli. The GeoClaw software for depth-averaged flows with adaptive refinement. 34(9):1195–1206, September 2011. doi: 10.1016/j.advwatres.2011.02.016. arXiv:1008.0455v2 [physics.geo-ph].

S. Bi, J. Zhou, Y. Liu, and L. Song. A finite volume method for modeling shallow flows with wet-dry fronts on adaptive cartesian grids. *Mathematical problems in Engineering*, 2014, 2014.

O. Bokhove. Flooding and drying in discontinuous galerkin finite-element discretizations of shallow-water equations. part 1: one dimension. *Journal of scientific computing*, 22(1):47–82, 2005.

A. Buttinger-Kreuzhuber, Z. Horváth, S. Noelle, G. Blöschl, and J. Waser. A fast second-order shallow water scheme on two-dimensional structured grids over abrupt topography. *Advances in water resources*, 127:89–108, 2019.

E. Chaabelasri, M. Jeyar, N. Salhi, and I. Elmahi. A simple unstructured finite volume scheme for solving shallow water equations with wet/dry interface. *International Journal of Mechanical Engineering and Technology*, 10(1):1849, 2019.

F. Dias and D. Dutykh. Dynamics of tsunami waves. In *Extreme man-made and natural hazards in dynamics of structures*, pages 201–224. Springer, 2007.

D. Dutykh and F. Dias. Water waves generated by a moving bottom. In *Tsunami and Nonlinear waves*, pages 65–95. Springer, 2007.

M. Fišer, I. Özgen, R. Hinkelmann, and J. Vimmr. A mass conservative well-balanced reconstruction at wet/dry interfaces for the godunov-type shallow water model. *International Journal for Numerical Methods in Fluids*, 82(12):893–908, 2016.

S. Gaudreault, M. Charron, V. Dallerit, and M. Tokman. High-order numerical solutions to the shallow-water equations on the rotated cubed-sphere grid. *arXiv preprint arXiv:2101.05617*, 2021.

D. L. George. Finite volume methods and adaptive refinement for tsunami propagation and inundation, 2006.

D. L. George. Augmented Riemann solvers for the shallow water equations over variable topography with steady states and inundation. *J Comp Phys*, 227(6):3089 – 3113, 2008. ISSN 0021-9991. doi: https://doi.org/10.1016/j.jcp.2007.10.027. URL http://www.sciencedirect.com/science/article/pii/S0021999107004767.

D. L. George. Adaptive finite volume methods with well-balanced Riemann solvers for modeling floods in rugged terrain: Application to the Malpasset dam-break flood (France, 1959). 66(8):1000–1018, 2011. ISSN 1097-0363. doi: 10.1002/fld.2298. URL http://dx.doi.org/10.1002/fld.2298.

S. K. Godunov. A difference scheme for numerical solution of discontinuous solution of hydrodynamic equations. *Math. Sbornik*, 47:271–306, 1959.

M. P. Hickey, G. Schubert, and R. Walterscheid. Propagation of tsunami-driven gravity waves into the thermosphere and ionosphere. *Journal of Geophysical Research: Space Physics*, 114(A8), 2009.

J. Hou, Q. Liang, F. Simons, and R. Hinkelmann. A 2d well-balanced shallow flow model for unstructured grids with novel slope source term treatment. *Advances in Water Resources*, 52:107–131, 2013.

J. Hou, Q. Liang, H. Zhang, and R. Hinkelmann. Multislope muscl method applied to solve shallow water equations. *Computers & Mathematics with Applications*, 68(12):2012–2027, 2014.

Y. Huang, N. Zhang, and Y. Pei. Well-balanced finite volume scheme for shallow water flooding and drying over arbitrary topography. *Engineering Applications of Computational Fluid Mechanics*, 7 (1):40–54, 2013.

E. J. Kubatko, J. J. Westerink, and C. Dawson. Semi discrete discontinuous galerkin methods and stage-exceeding-order, strong-stability-preserving runge–kutta time discretizations. *Journal of Computational Physics*, 222(2):832–848, 2007.

R. J. LeVeque and M. Pelanti. A class of approximate riemann solvers and their relation to relaxation schemes. *Journal of Computational Physics*, 172(2):572–591, 2001.

R. J. LeVeque, D. L. George, and M. J. Berger. Tsunami modelling with adaptively refined finite volume methods. 20:211 – 289, May 2011. doi: 10.1017/S0962492911000043.

R. J. LeVeque et al. *Finite volume methods for hyperbolic problems*, volume 31. Cambridge university press, 2002.

Q. Liang and A. G. Borthwick. Adaptive quadtree simulation of shallow flows with wet–dry fronts over complex topography. *Computers & Fluids*, 38(2):221–234, 2009.

D. Liu, J. Tang, H. Wang, Y. Cao, N. A. Bazai, H. Chen, and D. Liu. A new method for wet-dry front treatment in outburst flood simulation. *Water*, 13(2):221, 2021.

K. A. Lundquist, F. K. Chow, and J. K. Lundquist. An immersed boundary method for the weather research and forecasting model. *Monthly Weather Review*, 138(3):796–817, 2010.

K. T. Mandli. A numerical method for the two layer shallow water equations with dry states. *Ocean Modelling*, 72:80–91, 2013.

K. T. Mandli, A. J. Ahmadia, M. Berger, D. Calhoun, D. L. George, Y. Hadjimichael, D. I. Ketcheson, G. I. Lemoine, and R. J. LeVeque. Clawpack: Building an open source ecosystem for solving hyperbolic PDEs. 2(68), August 8 2016. doi: https://doi.org/10.7717/peerj-cs.68. URL `https://peerj.com/search/?q=mandli&t=&type=articles&subject=&topic=&uid=&sort=&journal=cs&discipline=&type=articles`.

F. Marche, P. Bonneton, P. Fabrie, and N. Seguin. Evaluation of well-balanced bore-capturing schemes for 2d wetting and drying processes. *International Journal for Numerical Methods in Fluids*, 53(5): 867–894, 2007.

P. McCorquodale, P. Ullrich, H. Johansen, and P. Colella. An adaptive multiblock high-order finite-volume method for solving the shallow-water equations on the sphere. *Communications in Applied Mathematics and Computational Science*, 10(2):121–162, 2015.

X. Meng, A. Komjathy, O. Verkhoglyadova, Y.-M. Yang, Y. Deng, and A. Mannucci. A new physics-based modeling approach for tsunami-ionosphere coupling. *Geophysical Research Letters*, 42(12): 4736–4744, 2015.

I. Nikolos and A. Delis. An unstructured node-centered finite volume scheme for shallow water flows with wet/dry fronts over complex topography. *Computer Methods in Applied Mechanics and Engineering*, 198(47-48):3723–3750, 2009.

M. Pelanti and F. Bouchut. A relaxation method for modeling two-phase shallow granular flows. In *Proceedings of Symposia in Applied Mathematics*, volume 67, pages 835–844, 2008.

M. Pelanti, F. Bouchut, and A. Mangeney. A riemann solver for single-phase and two-phase shallow flow models based on relaxation. relations with roe and vfroe solvers. *Journal of Computational Physics*, 230(3):515–550, 2011.

S. Popinet. Quadtree-adaptive tsunami modelling. *Ocean Dynamics*, 61(9):1261–1285, 2011.

S. Popinet. A quadtree-adaptive multigrid solver for the serre–green–naghdi equations. *Journal of Computational Physics*, 302:336–358, 2015.

P. L. Roe. Approximate riemann solvers, parameter vectors, and difference schemes. *Journal of computational physics*, 43(2):357–372, 1981.

C. Sánchez-Linares, M. de la Asunción, M. J. Castro, J. M. González-Vida, J. Macías, and S. Mishra. Uncertainty quantification in tsunami modeling using multi-level monte carlo finite volume method. *Journal of Mathematics in Industry*, 6(1):1–26, 2016.

G. Savastano, A. Komjathy, O. Verkhoglyadova, A. Mazzoni, M. Crespi, Y. Wei, and A. J. Mannucci. Real-time detection of tsunami ionospheric disturbances with a stand-alone gnss receiver: A preliminary feasibility demonstration. *Scientific reports*, 7(1):1–10, 2017.

L. Song, J. Zhou, J. Guo, Q. Zou, and Y. Liu. A robust well-balanced finite volume model for shallow water flows with wetting and drying over irregular terrain. *Advances in Water Resources*, 34(7): 915–932, 2011a.

L. Song, J. Zhou, Q. Li, X. Yang, and Y. Zhang. An unstructured finite volume model for dam-break floods with wet/dry fronts over complex topography. *International Journal for Numerical Methods in Fluids*, 67(8):960–980, 2011b.

E. F. Toro. *Shock-capturing methods for free-surface shallow flows*. Wiley-Blackwell, 2001.

B. Van Leer. Towards the ultimate conservative difference scheme. v. a second-order sequel to godunov's method. *Journal of computational Physics*, 32(1):101–136, 1979.

J. Zhao, I. Özgen-Xian, D. Liang, T. Wang, and R. Hinkelmann. An improved multislope muscl scheme for solving shallow water equations on unstructured grids. *Computers & Mathematics with Applications*, 77(2):576–596, 2019.